RSC Advances

PAPER

View Article Online
View Journal | View Issue



Cite this: *RSC Adv.*, 2025, **15**, 39672

# Solvent-free synthesis of amine-grafted adsorbent for direct air capture

Jinrui Li,[a] Nao Tsunoji *[ab] and Masahiro Sadakane [a]

Received 13th May 2025
Accepted 15th October 2025

DOI: 10.1039/d5ra03355a

rsc.li/rsc-advances

Amino-silane-grafted adsorbents were successfully synthesized by a solvent-free method. A silane solution was introduced into the pores of a porous silica support through capillary action and grafted by subsequent heating. Characterization of materials with different synthesis and pre-treatment conditions revealed that the pre-treatment to remove the water in the support and suitable amounts of silane were crucial factors to uniformly graft the amine on the porous support in the solvent-free method. Further, we investigated the $CO_2$ adsorption performance of amine-grafted materials in dry or humid 400 ppm $CO_2$ gases, demonstrating that the obtained materials synthesized by the solvent-free method exhibited good adsorption performance, comparable to that of conventional $CO_2$ adsorbents.



## Introduction

Direct air capture (DAC), a technology for directly and artificially capturing $CO_2$ from air, has gained considerable attention because of growing concerns about climate change and the demand for a sustainable society.[1,2] Amino-silane-grafted solid adsorbents are gathering momentum for DAC applications owing to their cycling stability, high energy efficiency, and merit against corrosion resistance.[1,3–5] Several types of amino-silane-grafted silica and other porous materials have been suggested by the Climeworks company for DAC systems.[6] In Climeworks' Orca plant, 3-aminopropylmethyldiethoxysilane-modified nano-fibrillated cellulose has been used, which can capture 4000 tons of $CO_2$ annually.[7] As of 2023, 18 DAC plants have been set up worldwide, and the total $CO_2$ capture capacity of these 18 plants is approximately 10 000 tons of $CO_2$ per year.[7] However, the Intergovernmental Panel on Climate Change indicates that in addition to reducing $CO_2$ emissions from industry, 2–20 gigatons of $CO_2$ need to be annually removed from the air by 2050.[8,9] Thus, DAC technology must become more economically feasible on a large scale to expand its deployment.[8]

One of the biggest obstacles to realizing cost-effective DAC is the cost of the adsorbent. Several cost analyses indicated the overall cost of DAC is sensitive not only to the performance but also purchase cost of DAC adsorbent.[2,6,10,11] The typical synthesis of amino-silane-grafted adsorbents requires excessive usage of amino silane, because a larger amount of amino silane increases the grafting efficiency on the surface of the support.[12] Recently, Li *et al.*[13,14] found that amino-silane-grafted adsorbents prepared by the impregnation method with the minimum silane usage exhibited excellent DAC performance, comparable to that of reported adsorbents prepared with excess silane. However, existing synthesis procedures, including the method reported by Li *et al.*,[13,14] still require the use of organic solvents. The separation and recycling of organic solvents is environmentally problematic, and it requires extra energy consumption and specific equipment.[15] Although the direct grafting of amino silane onto a porous support through mechano-chemical techniques has been reported, these synthesis methods require special equipment (*e.g.*, for ball milling) and another organic solvent for sample washing.[16,17]

Herein, we report a facile strategy for synthesizing an amino-silane-grafted adsorbent based on a solvent-free method that also minimizes the use of amino silane. By using the capillary action phenomenon of porous materials under suitable synthesis conditions, the pores of the support can be uniformly filled with amino silane liquid. Subsequently, amino silane is grafted on the support through a heat treatment. In this study, 3-aminopropyltrimethoxysilane (APTMS) was used as a silane coupling agent. The resulting amino-silane-grafted mesoporous silica by the solvent-free method [SBA-SF-X, X = amino silane addition (wt.%)] was synthesized by physical mixing. For comparison, we also synthesized APTMS-grafted SBA-15 by the impregnation method using an organic solvent (acetonitrile) [SBA-Imp(A)-X], according to the method reported by Li *et al.*[13,14] Considering the cost-effectiveness and environmental friendliness of water, we also conducted this impregnation synthesis using water instead of acetonitrile [SBA-Imp(W)-X]. We found that acetonitrile was a useful organic solvent to achieve a high $CO_2$ adsorption amount in the previous optimization study using the impregnation method.[13] For the SBA-Imp(W)-X samples, water was removed by vacuum drying at 70 °C. Finally, SBA-Heat(W)-X samples were synthesized by heating

[a]*Department of Applied Chemistry, Graduate School of Advanced Science and Engineering, Hiroshima University, Higashi-Hiroshima, 739-8527, Japan*
[b]*Center for Research on Green Sustainable Chemistry, Tottori University, 4-101 Koyama-cho Minami, Tottori 680-8552, Japan. E-mail: tsunoji@tottori-u.ac.jp*

and evaporation at 70 °C and atmospheric pressure for 2.5 days to remove the water. However, in this study, we regarded SBA-Imp(W)-X and SBA-Heat(W)-X as reference samples to obtain insights into the influence of water because these two samples exhibited lower DAC performance than other samples. X-ray diffraction (XRD), Fourier transform infrared (FT-IR), $^{29}$Si magic-angle spinning nuclear magnetic resonance spectroscopy ($^{29}$Si MAS NMR), $N_2$ adsorption–desorption, scanning electron microscopy (SEM), transmission electron microscopy (TEM) and CHN elemental analysis were employed to characterize the grafting of amino-silane. We also investigated the $CO_2$ adsorption property of the obtained amine-grafted materials using humid or dry 400 ppm $CO_2$ gases.

# Experimental

## Materials

Pluronic P123 ($EO_{20}PO_{70}EO_{20}$, Aldrich), tetraethyl orthosilicate (TEOS, Tokyo Chemical Co Inc.), HCl (36 wt.%, Fujifilm Wako Chemical Co), acetonitrile (99.8%, super dehydrated, Fujifilm Wako Chemical Co), 3-aminopropyltriethoxysilane (APTMS, 96%, Tokyo Chemical Co Inc.), *N*-[3-(trimethoxysilyl)propyl] ethylenediamine (97%, Aldrich) and 3-(trimethoxysilylpropyl) diethylenetriamine (technical grade, Aldrich).

## Synthesis of amino-silane-grafted mesoporous silica

The preparation of SBA-15 was based on a previous report.[13]

The amino-silane-grafted SBA-15 was synthesized as follows:

**SBA-SF-X.** SBA-15 (0.1 g) was added into a 15 ml Teflon test tube, and then, $N_2$ gas was continuously introduced into the tube, which was heated at 80 °C for 3 h to remove adsorbed water. After 3 h of the drying pretreatment, the SBA-15 was cooled down to room temperature in a $N_2$ environment, and APTMS was added into the Teflon test tube. Subsequently, the mixture was ground and stirred using a stirring rod in a $N_2$ environment at room temperature for 15 min. After grinding, $N_2$ flow was continuously introduced into the Teflon tube containing the mixture, which was heated at 80 °C for another 1 h.

**SBA-Imp(A)-X.** SBA-15 (0.3 g) was dispersed in 5 ml of acetonitrile containing a specified quantity of APTMS. This mixture was placed in a 15 ml Teflon test tube. The mixture was then dried for 24 h at 70 °C under atmospheric pressure to remove the solvent completely.

**SBA-Imp(W)-X.** SBA-15 (0.3 g) was dispersed in 5 ml of deionized water containing a certain quantity of APTMS, and the mixture was placed in a 15 ml Teflon test tube. The mixture was then vacuum dried at 70 °C for 1.5 h to remove water.

**SBA-Heat(W)-X.** SBA-15 (0.3 g) was dispersed in 5 ml of deionized water containing a specified quantity of APTMS. This mixture was then placed in a 15 ml Teflon test tube before heating to 70 °C at atmospheric pressure for 2.5 days until the water was completely removed.

APTMS was loaded onto SBA-15 *via* the condensation reaction shown in eqn (1), and the weight of the added amino-silane was calculated using eqn (2), taking into account the removal of methanol.

$$H_2NCH_2CH_2CH_2Si(OCH_3)_3 + 3\ R_3Si(OH) \rightarrow H_2NCH_2CH_2CH_2Si(OSiR_3)_3 + 3\ CH_3OH \quad (1)$$

$$\text{Amino silane addition(wt.\%)} = \frac{M_{\text{APTMS}} - M_{CH_3O^-}}{M_{\text{support}} + M_{\text{APTMS}} - M_{\text{MeOH}}} \quad (2)$$

where $M_{\text{APTMS}}$, $M_{\text{support}}$, $M_{CH_3O^-}$, and $M_{\text{MeOH}}$ correspond to the masses of APTMS, support, $CH_3O^-$ in APTMS, and methanol, respectively. All methoxy groups from APTMS were assumed to be converted into methanol.

**$CO_2$ adsorption measurement.** The $CO_2$ adsorption amount of the samples was measured by using a thermogravimetric analyzer (TGA). The samples were pretreated at 80 °C under $N_2$ gas flow for 30 min before cooling down to 30 °C. Then, dry 400 ppm $CO_2/N_2$ gas was introduced, and the $CO_2$ adsorption amount was calculated based on the mass change after introducing the $CO_2$-containing gas (Fig. S1, SI). In addition, the $CO_2$ adsorption performance was also test at 25 °C in 400 ppm $CO_2$/He gas with 60% relative humidity (Fig. S2, SI) through breakthrough instrument. More detailed about $CO_2$ adsorption measurement and structural characterization are listed in SI.

# Results and discussion

The XRD pattern (Fig. S3, SI) of SBA-15 exhibits diffraction peaks originating from the (100), (110), and (200) planes of the hexagonal structure of mesoporous silica. After grafting with APTMS, the peak intensity significantly decreased in SBA-Heat(W)-X especially in the sample with high addition of silane, while these peaks remained in the patterns of the other samples. The TEM (Fig. S4, SI) image of SBA-Heat(W)-30 lacks the contrast originating from an orderly arrangement of pores and walls. This structural degradation was attributed to the long-term hydrothermal treatment under alkaline conditions.[18,19]

The FT-IR spectrum (Fig. S5, SI) shows five peaks, attributed to the $NH_2$, CN, and $CH_2$ groups of grafted APTMS.[20] The $^{29}$Si MAS NMR spectra (Fig. S6, SI) display signals from APTMS and its grafting. Peaks related to the $T^2$ ($(SiO)_2SiOHOR$) and $T^3$ ($(SiO)_3SiOR$) sites of grafted APTMS appeared at −60 and −68 ppm, respectively. The CHN elemental analysis (Table S1) reveals that the actual amino silane loading increased with the increasing addition of amine. These analytical results indicate that APTMS was successfully grafted onto the support, while the mesoporous structure of SBA-15 was preserved in SBA-Imp(W)-X, SBA-Imp(A)-X, and SBA-SF-X.

Fig. 1 shows the $CO_2$ adsorption amount under dry conditions. Regardless of the amount of amino silane added, SBA-Heat(W)-X adsorbed a remarkably low amount of $CO_2$ because it lacked its original structure. For the other samples, the $CO_2$ adsorption amount increased in the range of 15–30 wt.% amino silane and then decreased above 35 wt.%. SBA-Imp(W)-X adsorbed less $CO_2$ than SBA-Imp(A)-X and SBA-SF-X at all amounts of amino silane. At the optimal amino silane addition (30 wt.%), SBA-SF-30 and SBA-Imp(A)-30 adsorbed similar amounts of $CO_2$ of 0.60 and 0.57 mmol $g^{-1}$, respectively, which

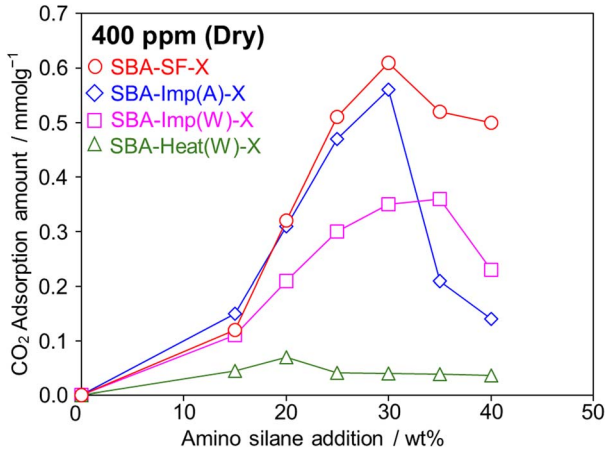


Fig. 1 $CO_2$ adsorption amounts of all samples in 400 ppm $CO_2$ under dry conditions measured by TGA.

are comparable to those of existing amino-silane-grafted adsorbents (Table S2, SI). However, for the SBA-SF-X with 35 wt.% amine or higher, the $CO_2$ adsorption remained high and did not decrease significantly, in contrast with the SBA-Imp(A)-X samples, implying that SBA-SF-X had more uniform grafting state. This is due to the uniform loading state of silane on SBA-SF materials, which provided their high BET surface area in the high loading level (Table S5). This $CO_2$ adsorption performance suggested that the cost-effective solvent-free method was an excellent approach for synthesizing adsorbents with high DAC performance.

To understand why the solvent-free method enabled high $CO_2$ adsorption even in the larger additions of amino silane, SEM, $N_2$ adsorption–desorption, and $^{29}$Si MAS NMR were conducted. Fig. 2 schematically illustrates the expected grafting processes of amino silane under different conditions. The SEM images (Fig. S7 and S8, SI) reveal that regardless of the synthesis

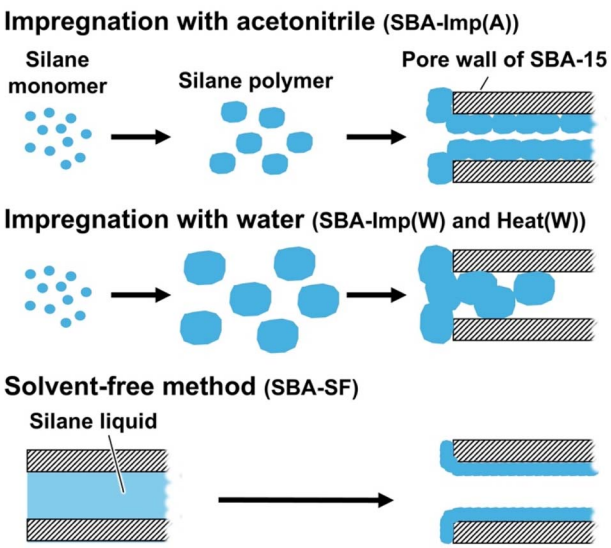


Fig. 2 Schematic of the APTMS modification process.

method, the morphology of the mesoporous silica particles did not significantly change from that of the original SBA-15. However, irregular particles with sizes of over 5 μm appeared in SBA-Imp(W)-30 and SBA-Heat(W)-30. $^{29}$Si MAS NMR (Fig. S6 and Tables S3–S4) demonstrated that the amount of surface silanol on SBA-15 consumed to prepare SBA-Imp(W)-30 was only 3.9%, suggesting that the majority of APTMS did not react with the surface silanol of SBA-15. Therefore, these enormous particles were concluded to be polymers formed by the intermolecular condensation of APTMS.

The detailed pore structures of the APTMS-grafted samples were measured by $N_2$ adsorption at −196 °C. The pore size distribution was evaluated through the Barrett–Joyner–Halenda (BJH) model from the adsorption branch (Fig. S9–S11 and Table S5, SI). After APTMS grafting, all samples had smaller pores than SBA-15 (5.4 nm). Notably, the BJH curves indicate that the SBA-SF-X samples retained a mesoporous structure with a pore size of 4.8 nm, even with aminol silane additions above 30 wt.%. In contrast, no mesopores were observed in the SBA-Imp(A)-X and SBA-Imp(W)-X samples at these levels of amine loading, indicating that the mesoporous structure of SBA-15 was completely blocked by APTMS. Thus, the high $CO_2$ adsorption amount of SBA-SF-X was considered to be related to its uniform pore size.

In a previously reported silane grafting process in solutions,[21] the main reaction was the hydrolysis of silane through existing water, which could be from the solvent or even from the air.[21,22] Subsequently, competitive reactions occurred: the intermolecular condensation of hydrolyzed silane in solution resulting in the formation of polymer and the heterogeneous condensation reaction of hydrolyzed silane with the silanol groups on the support surface. However, even using anhydrous organic solvents, the formation of silane polymer can't be inhibited completely.[22] In addition, because of the catalytic effect of $NH_2$ groups on the condensation of silane, amino silane inevitably forms polymers in organic solutions and modifies them onto the support in the form of polymers.[23,24] In aqueous solution, water promotes the intermolecular condensation reaction of amino silane, forming larger amino silane polymers,[25] which are difficult to incorporate into the mesopores of SBA-15.

To understand the modification process under solvent-free conditions, a sample wherein APTMS and SBA-15 were physically mixed without a heat treatment was characterized by XRD. The XRD pattern (Fig. S12, SI) shows that the intensity of the peak originating from the mesoporous structure significantly decreased just after mixing with APTMS. The disappearance of this peak was due to the APTMS liquid filling the mesopore spaces, which prevented X-ray scattering.[26,27] After the subsequent heat treatment, the XRD peak for SBA-15 increased in intensity (this state was used for the $CO_2$ adsorption experiment). Therefore, APTMS was introduced uniformly through the capillary action, and mesopore spaces were created by the heat treatment. The $^{29}$Si MAS NMR results (Table S4, SI) were not contradicted by this hypothesis. The surface silanol consumption of SBA-SF-X was 46.7%, indicating that the introduced APTMS actually condensed with the surface silanol

of SBA-15. In addition, the influence of the pre-drying treatment of SBA-15 was investigated, and the SBA-SF-X sample prepared using SBA-15 without pre-drying adsorbed less $CO_2$ than that synthesized with the pre-dried SBA-15 sample (Fig. S13, SI). Moreover, the $N_2$ adsorption measurements (Fig. S14 and Table S6, SI) revealed that the surface area and pore size of the SBA-SF-X sample without pre-drying were smaller than those of the SBA-SF-X sample prepared using pre-dried SBA-15.[25] Although XRD did not reveal a significant difference between the samples with or without pre-drying (Fig. S15), some irregular APTMS polymer particles appear in the SEM images of the sample without pre-drying (Fig. S16). These characteristics indicate that the presence of water in the pores hindered the capillary action of the APTMS polymer during solvent-free synthesis. Therefore, adjusting the addition of silane and the pre-drying treatment to remove water were both crucial to achieving solvent-free amino silane grafting.

To verify the versatility of the solvent-free method in this study, samples were also synthesized using *N*-[3-(trimethoxysilyl)propyl]ethylenediamine (diamine) and 3-(trimethoxysilylpropyl)diethylenetriamine (triamine), and their $CO_2$ adsorption performance was measured by TGA (Fig. S17, SI). The SBA-SF-X(diamine) and SBA-SF-X(triamine) adsorbed the highest $CO_2$ amounts of 0.68 and 0.48 mmol $g^{-1}$, respectively, when the amino silane addition was 30 wt.%. The results of TGA and the comparison with existing amino-silane-grafted adsorbents (Table S7, SI) confirm the wide applicability of the proposed synthesis method.

The recycling stability of the adsorbent is also a crucial parameter. Thus, the adsorption performance of the adsorbents during multiple cycles under dry and simulated DAC conditions was tested. Fig. 3 shows that during five cycles under dry conditions (in TGA), both SBA-Imp(A)-30 and SBA-SF-30 maintained stable adsorption amounts of 0.56 and 0.60 mmol $g^{-1}$, respectively. In the humid environment, the average $CO_2$ adsorption of SBA-Imp(A)-30 and SBA-SF-30 during five cycles was 0.33 and 0.38 mmol $g^{-1}$, respectively, which were slightly lower than those under dry conditions. Under humid conditions, the initial adsorption amount of SBA-SF-30 was relatively low (0.27 mmol $g^{-1}$); however, from the second cycle, the adsorption amount of SBA-SF-30 increased (0.40 mmol $g^{-1}$) and remained stable in subsequent cycles. In contrast, the adsorption amount of SBA-Imp(A)-30 gradually decreased during multiple cycles. Although $^{29}$Si MAS NMR showed that modification states of APTMS in SBA-Imp(A)-30 and SBA-SF-30 were similar, the pores of SBA-SF-30 (4.8 nm) were larger than those of SBA-Imp(A)-30 (4.2 nm). Thus, this difference of the $CO_2$ adsorption amount between SF and Imp(A) samples was probably related to the competitive adsorption of water reported previously.[28] Some research groups have proposed that the presence of water can block adsorbent pores.[29] Thus, the uniformly large pore structure of SBA-SF-30 may have played an important role in its high stability.

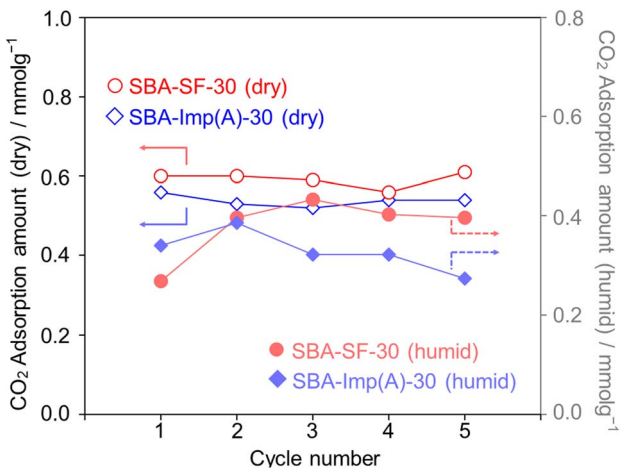


Fig. 3 Recycle stability of SBA-Imp(A) and SBA-SF-30 under simulated dry and humid DAC conditions.

## Conclusions

We demonstrated that amino-silane-grafted adsorbents could be prepared by a solvent-free method that minimized amino silane usage. The obtained SBA-SF-30 with a uniform pore structure adsorbed 0.6 mmol $g^{-1}$ $CO_2$ under dry 400 ppm $CO_2$ conditions, and this adsorbent showed excellent stability in both dry and humid DAC environments. Additionally, different silanes could be used in this method. This work offers good prospects for the efficient, cost-effective synthesis of amino-silane-grafted adsorbents for deploying DAC technologies on a large scale, and it provides new insights into the synthesis of various $CO_2$ adsorbents.

## Author contributions

Jinrui Li conceptualization, data curation, investigation, writing-original draft; Nao Tsunoji conceptualization, funding acquisition, resources, supervision, validation, writing – review & editing; Masahiro Sadakane funding acquisition, resources, supervision, writing-review & editing.

## Conflicts of interest

There are no conflicts to declare.

## Data availability

The data supporting this article have been included as part of the supplementary information (SI). Supplementary information: experimental methods, characterization data (XRD, TEM, FT-IR, NMR, SEM, $N_2$ adsorption–desorption, and CHN elemental analysis), $CO_2$ adsorption curves, and performance comparison. See DOI: https://doi.org/10.1039/d5ra03355a.

## Acknowledgements

We are grateful for financial support from the New Energy and Industrial Technology Development Organization (NEDO) through project JPNP20004, and the Feasibility Study Program

(Uncharted Territory Challenge 2050) JPNP14004. Additional support was provided by the JST SICORP program (Grant Number JPMJSC22C5), JST SPRING (Grant Number JPMJSP2132) and JSPS KAKENHI (Grant Numbers 22H01868, 25K01582, 23K21059, and 23H05454).

## Notes and references

1 L. Jiang, W. Liu, R. Q. Wang, A. Gonzalez-Diaz, M. F. Rojas-Michaga, S. Michailos, M. Pourkashanian, X. J. Zhang and C. Font-Palma, *Prog. Energy Combust. Sci.*, 2023, **95**, 101069.
2 X. Shi, H. Xiao, H. Azarabadi, J. Song, X. Wu, X. Chen and K. S. Lackner, *Angew. Chem., Int. Ed.*, 2020, **59**, 6984–7006.
3 Y. Fan and X. Jia, *Energy Fuels*, 2022, **36**, 1252–1270.
4 J.-T. Anyanwu, Y. Wang and R. T. Yang, *Chem. Eng. Sci.*, 2022, **254**, 117626.
5 F. Sabatino, A. Grimm, F. Gallucci, M. van Sint Annaland, G. J. Kramer and M. Gazzani, *Joule*, 2021, **5**, 2047–2076.
6 G. Leonzio, P. S. Fennell and N. Shah, *Appl. Sci.*, 2022, **12**, 2618.
7 O. Al Yafiee, F. Mumtaz, P. Kumari, G. N. Karanikolos, A. Decarlis and L. F. Dumée, *Chem. Eng. J.*, 2024, 154421.
8 M. Ozkan, S. P. Nayak, A. D. Ruiz and W. Jiang, *Iscience*, 2022, **25**, 103990.
9 V. Masson-Delmotte, P. Zhai, H.-O. Pörtner, D. Roberts, J. Skea, P. R. Shukla, A. Pirani, W. Moufouma-Okia, C. Péan, R. Pidcock, S. Connors, J. B. R. Matthews, Y. Chen, X. Zhou, M. I. Gomis, E. Lonnoy, T. Maycock, M. Tignor and T. Waterfiel, *Global Warming of 1.5 °C*, IPCC, 2018, **https://www.ipcc.ch/sr15/**.
10 H. A. Patel, J. Byun and C. T. Yavuz, *ChemSusChem*, 2017, **10**, 1303–1317.
11 A. Sinha, L. A. Darunte, C. W. Jones, M. J. Realff and Y. Kawajiri, *Ind. Eng. Chem. Res.*, 2017, **56**, 750–764.
12 N. N. Linneen, R. Pfeffer and Y. S. Lin, *Chem. Eng. J.*, 2014, **254**, 190–197.
13 J. Li, N. Tsunoji, R. Kumar, N. C. Sukmana and M. Sadakane, *J. Porous Mater.*, 2024, **31**, 1289–1304.
14 J. R. Li, N. Tsunoji, M. Bandyopadhyay and M. Sadakane, *Langmuir*, 2024, **40**, 22283–22289.
15 S. L. James, C. J. Adams, C. Bolm, D. Braga, P. Collier, T. Friščić, F. Grepioni, K. D. M. Harris, G. Hyett, W. Jones, A. Krebs, J. Mack, L. Maini, A. G. Orpen, I. P. Parkin, W. C. Shearouse, J. W. Steed and D. C. Waddell, *Chem. Soc. Rev.*, 2012, **41**, 413–447.
16 A. P. Amrute, B. Zibrowius and F. Schüth, *Chem. Mater.*, 2020, **32**, 4699–4706.
17 N. Celik, B. Sezen, F. Sahin, A. Ceylan, M. Ruzi and M. S. Onses, *ACS Appl. Nano Mater.*, 2023, **6**, 14921–14930.
18 M. Sun, X. Gao, Z. Zhang, C. Zou, D. Xin and G. Geng, *J. Am. Ceram. Soc.*, 2023, **106**, 6586–6601.
19 W. Li, P. Bollini, S. A. Didas, S. Choi, J. H. Drese and C. W. Jones, *ACS Appl. Mater. Interfaces*, 2010, **2**, 3363–3372.
20 N. Sosa, N. Chanlek and J. Wittayakun, *Ultrason. Sonochem.*, 2020, **62**, 104857.
21 S. Gauthier, J. P. Aimé, T. Bouhacina, A. J. Attias and B. Desbat, *Langmuir*, 1996, **12**, 5126–5137.
22 M. Zhu, M. Z. Lerum and W. Chen, *Langmuir*, 2012, **28**, 416–423.
23 Y. Millot, A. Hervier, J. Ayari, N. Hmili, J. Blanchard and S. Boujday, *J. Am. Chem. Soc.*, 2023, **145**, 6671–6681.
24 J. S. Manzano, H. Wang, T. Kobayashi, P. Naik, K. C. Lai, J. W. Evans and I. I. Slowing, *Micropor. Mesopor. Mater.*, 2020, **305**, 110276.
25 F. Bauer, S. Czihal, M. Bertmer, U. Decker, S. Naumov, S. Wassersleben and D. Enke, *Micropor. Mesopor. Mater.*, 2017, **250**, 221–231.
26 M. Laghaei, M. Sadeghi, B. Ghalei and M. Dinari, *Prog. Org. Coat.*, 2016, **90**, 163–170.
27 C. F. Holder and R. E. Schaak, *Journal*, 2019, **13**, 7359–7365.
28 J. Wang, S. Wang, Q. Xin and Y. Li, *J. Mater. Chem. A*, 2017, **5**, 6794–6816.
29 A. Kumar, D. G. Madden, M. Lusi, K. J. Chen, E. A. Daniels, T. Curtin, J. J. Perry IV and M. J. Zaworotko, *Angew. Chem., Int. Ed.*, 2015, **54**, 14372–14377.